DOI: 10.1021/ma902186e

Macromolecules
ARTICLE

Macromolecular Diffusion in Self-Assembling Biodegradable Thermosensitive Hydrogels

Tina Vermonden,*[,†,‡] Sidhartha S. Jena,[‡,§] David Barriet,[‡] Roberta Censi,[†] Jasper van der Gucht,[∥] Wim E. Hennink,[†] and Ronald A. Siegel[‡,⊥]

[†]*Department of Pharmaceutics, Utrecht Institute for Pharmaceutical Sciences, Utrecht University, P.O. Box 80082, 3508 TB, Utrecht, The Netherlands,* [‡]*Department of Pharmaceutics, University of Minnesota, Minneapolis, Minnesota 55455,* [§]*Department of Physics, National Institute of Technology, Rourkela, Rourkela 769008, Orissa, India,* [∥]*Laboratory of Physical Chemistry and Colloid Science, Wageningen University, Dreijenplein 6, 6703 HB Wageningen, The Netherlands, and* [⊥]*Department of Biomedical Engineering, University of Minnesota, Minneapolis, Minnesota 55455*

Received October 2, 2009; Revised Manuscript Received November 9, 2009

ABSTRACT: Hydrogel formation triggered by a change in temperature is an attractive mechanism for *in situ* gelling biomaterials for pharmaceutical applications such as the delivery of therapeutic proteins. In this study, hydrogels were prepared from ABA triblock polymers having thermosensitive poly(*N*-(2-hydroxypropyl)methacrylamide lactate) flanking A-blocks and hydrophilic poly(ethylene glycol) B-blocks. Polymers with fixed length A-blocks (∼22 kDa) but differing PEG-midblock lengths (2, 4, and 10 kDa) were synthesized and dissolved in water with dilute fluorescein isothiocyanate (FITC)-labeled dextrans (70 and 500 kDa). Hydrogels encapsulating the dextrans were formed by raising the temperature. Fluorescence recovery after photobleaching (FRAP) studies showed that diffusion coefficients and mobile fractions of the dextran dyes decreased upon elevating temperatures above 25 °C. Confocal laser scanning microscopy and cryo-SEM demonstrated that hydrogel structure depended on PEG block length. Phase separation into polymer-rich and water-rich domains occurred to a larger extent for polymers with small PEG blocks compared to polymers with a larger PEG block. By changing the PEG block length and thereby the hydrogel structure, the mobility of FITC-dextran could be tailored. At physiological pH the hydrogels degraded over time by ester hydrolysis, resulting in increased mobility of the encapsulated dye. Since diffusion can be controlled according to polymer design and concentration, plus temperature, these biocompatible hydrogels are attractive as potential *in situ* gelling biodegradable materials for macromolecular drug delivery.

Introduction

Hydrogels are cross-linked polymer networks that have the capacity to retain large quantities of water resulting in tissue-mimicking properties in which nutrients and drugs can diffuse in and out.[1] Cross-links may be either chemical, i.e. due to covalent linkages between monomer units on different chains, or physical, with chains linked by weaker forces such as hydrogen bonding, ionic bonding, hydrophobic interactions, inclusion complexes, or topological entanglements.[1−7] Hydrogels are also classified as permanent or degradable, where degradation is due to uncatalyzed or enzyme-catalyzed hydrolysis of chain units or cross-links.

Permanent, chemically cross-linked hydrogels are advantageous insofar as they resist creep deformation, but they are difficult to process. Difficulties in extracting unreacted monomer and initiator increases the toxic potential of chemically cross-linked hydrogels. Also, cross-linking agents might react with loaded proteins and other bioactives. For these reasons, aqueous polymer solutions that transform into physical gels in response to changes in environmental conditions such as temperature and pH have received much attention.[5,8−13] Such hydrogels can be formed *in situ*, and under proper conditions they can also entrap small and large molecules or even cells. Diffusion in reversible hydrogels can be controlled by appropriately tuning external environmental conditions.[14,15] For drug delivery applications, *in situ* formation and controlled diffusivity of molecules in reversible hydrogels provide a dual benefit.

Thermosensitive hydrogels having LCST (lower critical solution temperature) behavior are ideal candidates as injectable biomaterials because of easy mixing of the polymer solution with drugs or therapeutic proteins at low temperature. Upon injection and increase of temperature to 37 °C, a gel is formed *in situ*, encapsulating the drugs in the formed network.[16,17]

We have designed a class of self-assembling thermosensitive and biodegradable triblock polymers that undergo triggered hydrogelation with increased temperature.[5] The ABA triblock polymers consist of a hydrophilic PEG (B) middle block and thermosensitive poly(*N*-(2-hydroxypropyl)methacrylamide mono/dilactate) flanking (A)-blocks. The strength of the hydrogels can be tailored by polymer concentration, polymer block lengths, and temperature.[5,18] The temperature at which self-assembly of the thermosensitive A-blocks commences depends on the average length of the lactate side chains in these blocks.[19] The lactate groups are also responsible for the biodegradability of the hydrogel networks, as their ester bonds hydrolyze over time in physiological conditions,[20] yielding more hydrophilic polymers and therefore an increase in gel temperature, ultimately leading to dissociation of the network at 37 °C.

In this study, diffusion of encapsulated fluorescently labeled dextran dyes in the ABA triblock polymer hydrogels was assessed by fluorescence recovery after photobleaching (FRAP).[21]

*Corresponding author: e-mail T.Vermonden@uu.nl; Ph 0031-302537304; Fax 0031-302517839.

 Published on Web 11/25/2009

Temperature, the length of the PEG midblocks of the polymers, and hydrogel degradation time were varied to establish the potential use of these materials as drug delivery matrices. Results were correlated with rheological studies, confocal microscopy, cryo-SEM, and dye release over time.

In FRAP experiments, a thin layer of hydrogel containing a fluorescent probe is mounted on the stage of a fluorescence microscope. A transient, intense pulse of laser light applied to a cylindrical spot in the hydrogel defined by the microscope optics, bleaching fluorescent probe molecules within the spot. Following the pulse, fluorescence intensity of the spot is interrogated by the same optics, but at much reduced illumination. Extent and kinetics of fluorescence recovery in the spot provide information regarding diffusional exchange of probe molecules between the spot and its surroundings. Incomplete recovery of fluorescence indicates that a fraction of probe molecules is immobilized in the hydrogel. While FRAP has been used previously to quantify macromolecular diffusion in polyelectrolyte solutions,[22−24] covalently cross-linked hydrogels,[18,25−27] and biological tissues,[28,29] it has not been so extensively used to assess diffusion in reversible or biodegradable hydrogels.[30]

Materials and Methods

Materials. All commercial chemicals were obtained from Aldrich unless indicated otherwise and were used as received. L-Lactide was obtained from Purac Biochem BV (Gorinchem, The Netherlands). Hydroxypropylmethacrylamide monolactate (HPMAm-ML) and HPMAm dilactate were synthesized according to a previously described method.[20] Fluorescein isothiocyanate (FITC)-labeled dextrans with molecular weights of 70 and 500 kDa (FD70 and FD500) were obtained from Sigma-Aldrich.

Polymer Synthesis. Thermosensitive ABA triblock polymers were prepared according to a previously described procedure.[5] 4,4′-Azobis(4-cyanopentanoic acid) (ABCPA, obtained from Fluka) was used to prepare $(PEG\text{-}ABCPA)_n$ macroinitiators with PEG molecular weights 2000, 4000, or 10000 Da.[31] These initiators (66, 132, and 330 mg for 2000, 4000, and 10000 $(PEG-ABCPA)_n$, respectively) were used to copolymerize HPMAm monolactate (409 mg, 1.9 mmol) and HPMAm dilactate (1.64 g, 5.7 mmol) to obtain triblock polymers with polyHPMAm lactate as outer blocks (A-blocks) and PEG as the middle block (B-block).[31] Total yield was 1.5−1.8 g (70−80%) for each polymer.

Gel Permeation Chromatography. The molecular weights of the polymers were determined by GPC using a Plgel 5 μm MIXED-D column (Polymer Laboratories) with column temperature 40 °C. DMF containing 10 mM LiCl was used as eluent with an elution rate of 0.7 mL/min, and the sample concentration was ~5 mg/mL in the same eluent. Poly(ethylene glycol)s with defined molecular weights were used as standards.

^{1}H NMR Spectroscopy. Polymers dissolved in $CDCl_3$ were characterized by ^{1}H NMR on a Varian Mercury Plus 300 spectrometer. Chemical shifts were referred to the solvent peak (δ = 7.24 ppm for $CHCl_3$).

Cloud Point Measurements. Cloud points of the polymers were measured by static light scattering using a Horiba Fluorolog fluorimeter (650 nm, 90° angle) with heating rate of 1 °C/min. Polymers were dissolved at a concentration of 2 mg/mL in ammonium acetate buffer (pH 5.0, 120 mM). Cloud point was defined as the temperature of onset of increased scattering intensity.

Hydrogel Preparation. The polymers were dissolved at the indicated concentrations (20 or 30 wt %) in either ammonium acetate buffer (pH 5, 150 mM) or HEPES buffer (pH 7.5, 100 mM), both containing 0.02% NaN_3. pH 5 was chosen to minimize polymer degradation (ester hydrolysis) in time, and pH 7.5 was chosen to mimic physiological pH. The polymers were allowed to dissolve at 4 °C overnight. Hydrogels formed spontaneously when the samples were heated above the cloud point. Concentration of FD70 and FD500 was 2.0 mg/mL for gels at pH 5 and 0.2 mg/mL for gels at pH 7.5. Different concentrations of FD were necessary due to the pH dependence of fluorescence intensity of FITC derivatives.[32]

FRAP Apparatus. FRAP instrumentation consisted of a tunable argon ion laser (model 95-3, Lexel), a photomultiplier tube (PMT; model S982, Hamamatsu), an acousto-optical modulator (AOM; model N35085-3, Neos Technologies), neutral density filters (NDF's), and a fluorescence microscope equipped with an XYZ heating stage (Nikon Labphot 2), all mounted on an optical table (model RS-1000, Newport Instruments) with vibration isolating legs (model I-2000, Newport) and shielded from extraneous light by a curtain.

The laser beam, operating at 488 nm, was delivered through the AOM, NDF's, and an iris at the rear of the microscope. Stability was checked by deflecting part of the excitation beam to a photodetector (model 822, Newport) using a pellicle beam splitter (model 37400, Oriel). Fluorescence photoemissions were collected through the microscope optics and sent to the PMT through a dichroic mirror, which filtered out light below 510 nm. Photocurrent was converted to voltage across a 94 KΩ shunt resistor inserted between the positive and ground terminals of the PMT. Voltage was amplified (model SR560 preamplifier, Stanford Research Systems), digitized (PCI-MIO-16E4 multifunction PCI board, National Instruments), and stored on a PC for later analysis using Labview (National Instruments).

FRAP Measurements. Samples were prepared by pipeting polymer solutions in a cold room (4 °C) into flat capillaries (Microslides catalog no. W3520-100, 0.2 × 4.0 i.d., from ViroCom, Inc.). Filled capillaries were attached to microscope slides and placed on the mobile stage of fluorescence microscope. Sample temperature was set and controlled by a Peltier heater, and thermal equilibration was carried out for at least 15 min before FRAP measurements were started.

To initiate a FRAP measurement an intense, a 500 ms laser pulse bleached a cylindrical spot of radius 50 μm (r_0), with size controlled by the microscope's iris. This pulse was long enough to ensure adequate bleaching but short enough to obviate significant probe diffusion during the bleaching period. Following the bleaching pulse the beam was immediately attenuated by a factor of $10^{4.4}$ using the AOM and NDF's. The attenuated beam was shuttered on for 250 ms intervals, separated by 4.75 s periods during which the laser was completely blocked. Photoemission intensity data were gathered and integrated during the "on" periods over 10 min following the bleaching pulse. Just before each bleaching pulse, the spot was interrogated by the attenuated beam for 60 s in order to confirm that the latter did not bleach the sample and to establish a reference against which intensities recorded after photobleaching could be compared.

Between measurements for a given hydrogel, the XY position of the spot was moved or the temperature was changed. At least 15 min was allowed for thermal re-equilibration between these changes.

Analysis of FRAP Data. The fluorescence recovery voltage, $F(t)$, was normalized by its unbleached value, F_0, recorded just before the bleaching pulse. The resulting curve, $f(t) = F(t)/F_0$, was fit to a recovery function[21,33] that takes into account the cylindrical geometry of the bleached area and the beam's Gaussian profile

$$f(t) = f_1 + f_2 \exp\left(-\frac{2}{1+2t/\tau}\right) \quad (1)$$

where τ is the recovery time constant and f_1 and f_2 are constant coefficients related to bleach depth and the fraction of probe molecules that are mobile and can participate in recovery. With

data fit to eq 1, the diffusion coefficient of mobile probe, D, was calculated as[21]

$$D = \frac{r_0^2}{4\tau} \quad (2)$$

The mobile fraction, R, was obtained by

$$R = \frac{f^\infty - f^0}{1 - f^0} \quad (3)$$

where f^0 is the normalized fluorescence intensity immediately after bleaching and f^∞ is the normalized fluorescence intensity infinite time after bleaching.[25]

Bleach depth, $1 - f^0$, was set between 0.6 and 0.8 in order to achieve a proper fit of eq 1 to recovery data with good signal-to-noise ratio. For each sample, measurements performed at three XY positions were used to produce average values of D and R. Generally, coefficients of variation for these parameters, determined from three curves measured under each condition, were of order 15%. However, several of the recovery curves were very flat, indicating severely restricted probe mobility. In such cases it was not possible to obtain reliable estimates of f_1, f_2, and τ in eq 1, and D could not be identified, so they were not reported.

Rheological Characterization. Rheological analysis of the hydrogels was performed on an AR-G2 rheometer (TA-Instruments) equipped with a Peltier plate for temperature control using a cone−plate geometry (steel, 20 mm diameter with an angle of 1°). A solvent trap was used to prevent evaporation of the solvent. Unless otherwise indicated, a strain of 1% and a frequency of 1 Hz were used.

Confocal Laser Scanning Microscopy (CLSM). Confocal images were taken with a Zeiss Exciter confocal scanning system equipped with a 100× oil immersion objective (NA 1.46). Excitation wavelength was 514 nm (Ar laser). Pinhole settings were adjusted to obtain a slice thickness of 0.4 μm. Quick heating: transferring sample from the fridge immediately in a 50 °C water bath for 1 min and subsequently cooling to room temperature. Slow heating: transferring sample from fridge to room temperature.

Cryo-SEM. Scanning electron microscopy images were taken using a field emission gun HR-SEM (Hitachi S900) with an in lens design. The microscope was equipped with a Gatan model 626 cryostage. In order for the images of the sample to represent accurately the native state of the gel, a rapid freezing technique was used, high-pressure freezing, that relies on the rapid cooling of a thin sample sandwiched between Cu planchets using a liquid nitrogen jet. Our sample preparation was based on the work of Apkarian et al.[34] Briefly, in a cold room (4 °C) a microdroplet of sample was sandwiched between two Cu planchets (the cavity defined by the planchet assembly was 200 μm thick for a diameter of 2 mm). This assembly was mounted onto the high-pressure freezer sample holder. To prevent the sample chamber of the high-pressure freezer unit (Balzer HPM 010) from accumulating frost, a constant water flow was maintained around it while the liquid nitrogen jet was off. This water recirculation was used to equilibrate the sample at a given temperature for 5 min before turning the jet on. After pressure freezing, the planchet assembly was either kept under liquid nitrogen for storage or split open using a prechilled scalpel. All further operations were accomplished under liquid nitrogen to prevent ice formation on the sample. The planchet was then loaded onto the Gatan cryostage and the stage introduced within the high-vacuum environment of a Balzer MED 010 turbo mini deposition system. The sample was etched for 2 min at −115 °C to evaporate water from the gel and then returned to −160 °C to evaporate 2 nm of Pt on top of the etched sample. The sample was returned to liquid nitrogen temperature, removed from the high-vacuum environment, and quickly transferred to the SEM to limit the formation of frost. The microscope was operated under high-vacuum conditions ($< 10^{-7}$ Torr) at 3 kV to minimize beam damage on the sample.

Swelling/Degradation Studies. Hydrogels of 20 or 30 wt % with a total weight of ~200 mg were prepared in 1 mL glass vials as described above. Exact weights of the gels were measured (W_0). After incubating the gels at 37 °C for 1 h in a water bath, 0.6 mL of buffer (ammonium acetate 150 mM pH 5 or HEPES buffer 150 mM pH 7.5) was added. At regular intervals the incubation buffer was removed, and the gel weight (W_t) was measured to calculate the swelling ratio (SR = W_t/W_0). After each measurement, 0.6 mL of fresh buffer was placed on top of the hydrogel.

Results and Discussion

Polymer Characteristics. ABA triblock polymers with thermosensitive pHPMAm-lac A-blocks of ~22 kDa and hydrophilic PEG B-blocks with varying molecular weights of 2, 4, and 10 kDa (designated P2K, P4K, and P10K, respectively, as shown in Scheme 1) were synthesized by radical polymerization using $(PEG-ABCPA)_n$ as macroinitiator. The monomer feed ratio of HPMAm monolactate and HPMAm dilactate corresponded to the ratio found in the A-blocks of the polymers, which was 25/75 for all polymers as determined by ^{1}H NMR. Cloud points for all triblock polymers were close to 16 °C.[19]

Table 1 shows molecular weights of the polymers as measured by ^{1}H NMR and GPC. As reported earlier, the molecular weights obtained by GPC are lower than values derived from NMR, probably because the GPC standards

Scheme 1. Chemical Structures of Thermosensitive ABA Triblock Polymers

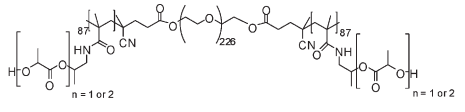

23- **10**- 23 kDa **P10K**

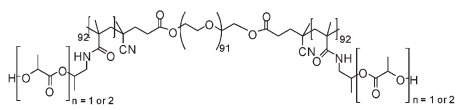

24- **4**- 24 kDa **P4K**

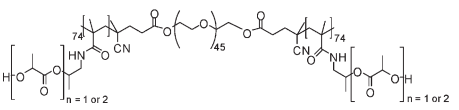

20- **2**- 20 kDa **P2K**

(PEG homopolymers) display relatively larger hydrodynamic volumes compared to our triblock polymers in the mobile phase.[5]

Macromolecular Diffusion in Hydrogels. Hydrogels were readily formed by dissolving the polymer at temperatures below the cloud point and subsequent heating to temperatures above the cloud point. To show that these hydrogels are suitable for entrapment of macromolecules, fluorescently labeled dextrans (FITC-Dextran) with different molecular weights (FD70 and FD500 having molecular weights of 70 and 500 kDa, respectively) were mixed with the polymer solutions at low temperature. Diffusion of these probes was followed by FRAP, with the hydrogels exposed to stepwise increases in temperature.

Figure 1 displays raw FRAP data for FD70 dye diffusing in 20 wt % P4K gel at different temperatures. Fluorescence recovery curves were fitted to eq 1, and values of R and D were calculated from eqs 2 and 3 and plotted in parts a and b of Figure 2, respectively. At 25 °C, fluorescence recovered completely within 10 min. Total recovery (R), reflecting the mobile fraction of dye, decreased with increasing temperature above 25 °C. Hardly any recovery occurred above 35 °C. A slight presently unexplained decrease in recovery was also observed sometimes below 25 °C.

With increasing temperature, a decrease in dye diffusion coefficient (D) was observed, reflecting gel formation with increasing temperature. Gel formation and related changes in dye mobility were completely reversible; R and D regained their former values when temperature was decreased (see Supporting Information).

Besides temperature, the polymer concentration and the size of the dye influenced the diffusion coefficients and mobile fraction. With increasing size of the dye, the diffusion coefficient and mobile fraction dropped. For example, $D = (13.8 \pm 1.5) \times 10^{-8}$ cm^2/s and $R = 94.4 \pm 4.9\%$ for FD70 and $D = (4.4 \pm 0.7) \times 10^{-8}$ cm^2/s and $R = 40.6 \pm 1.5\%$ for FD500 at 25 °C in 20 wt % P4K gels. Diffusion coefficient and mobile fraction also decreased with increasing polymer concentration, as expected ($D = (4.4 \pm 0.7) \times 10^{-8}$ cm^2/s and $R = 40.6 \pm 1.5\%$ for 20 wt % P4K gels to $D = (1.7 \pm 0.7) \times 10^{-8}$ cm^2/s and $R = 27.5 \pm 2.5\%$ for 30 wt % P4K gels at 25 °C for FD500).

Parts A and B of Figure 3 display fluorescence recovery curves for FD500 and FD70, respectively, in hydrogels formed with different PEG block lengths at constant polymer concentration and temperature. As above, the recovery and diffusion coefficients for the smaller dye (FD70) were greater than those for the larger dye (FD500). Large differences can also be seen between the different polymer gels. Gels prepared with polymers having the smallest PEG middle blocks (P2K) exhibited the highest recovery and diffusion coefficients. Fluorescence recovery decreased with increasing PEG midblock length. Apparently, the gel structure and pore size of the gels are highly dependent on the length of the hydrophilic PEG middle block, and this provides a means for tailoring transport properties. Thus, the rate of diffusion of the dextrans could be tailored by triblock polymer architecture.

Mechanical Properties of Hydrogels. Rheological properties of P10K hydrogels were reported in a previous paper.[5] A typical curve for the storage (G') and loss (G'') modulus as a function of temperature is shown in Figure 4A. At low temperatures the samples behave as viscous solutions, and upon raising the temperature a gel is formed. The temperature at which G' crosses G'', which can be seen as a rough estimate for the gel point, T_{gel}, decreases with increasing polymer concentration.

In Figure 4B, storage moduli of the hydrogels differing in PEG middle block length are shown at 20 and 37 °C. From this figure it is clear that polymers having shorter PEG middle blocks yield stronger gels. Although the weight

Table 1. Characteristics of Triblock Polymers

name	M_n (kDa)[a] A−B−A blocks	M_n (kDa)[b]	M_w (kDa)[b]	PDI[b]	CP (°C)[c]
P2K	20−2−20	27	51	1.9	15.8
P4K	24−4−24	27	55	2.0	16.1
P10K	23−10−23	43	67	1.6	16.2

[a] Determined by ^{1}H NMR. [b] Determined by GPC. [c] Cloud point (CP) measured by SLS for 2 mg/mL solution in 120 mM ammonium acetate buffer pH 5.0.

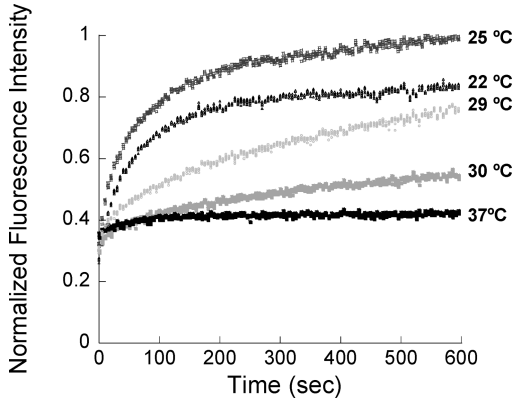

Figure 1. Normalized fluorescence recovery curves as a function of time for FD70 probe molecules in a 20 wt % P4K hydrogel at different temperatures at pH 7.5.

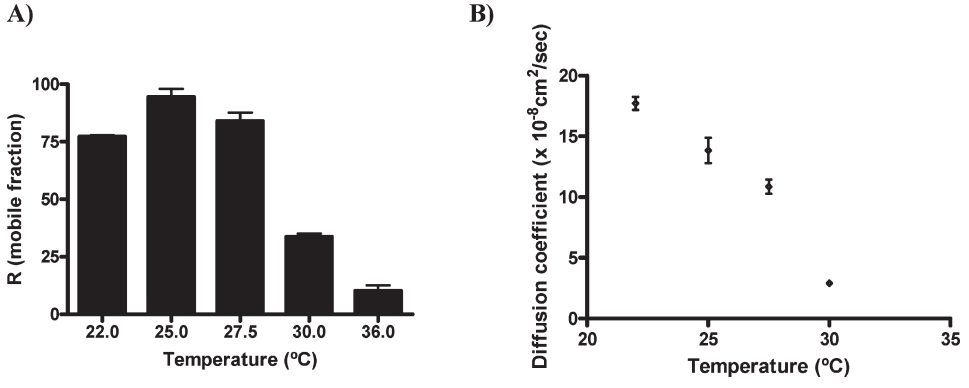

Figure 2. Mobile fraction (A) and diffusivity (B) calculated from fitted FRAP recovery curves of FD70 in 20 wt % P4K hydrogel at pH 7.5 as a function of temperature. Data are shown as mean ± standard deviation; $n = 3$.

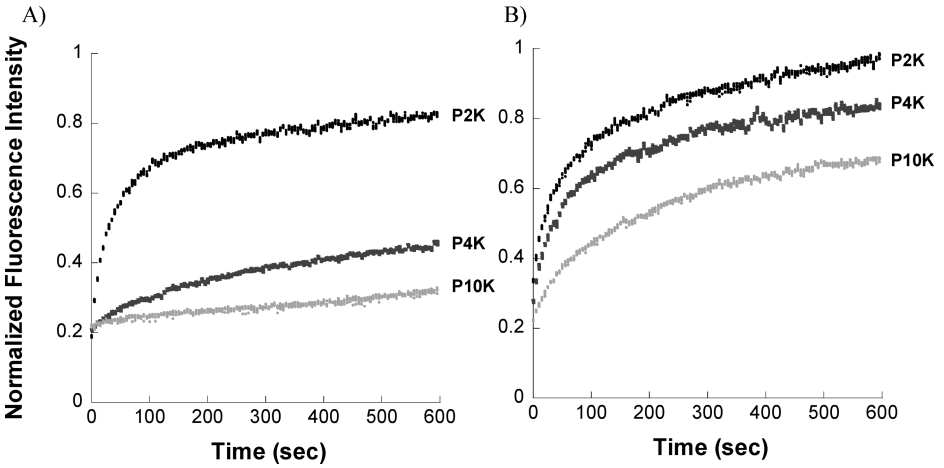

Figure 3. Fluorescence recovery curves of FD500 (A) and FD70 (B) (pH 5, 25 °C) in 30 wt % hydrogels of polymers differing in PEG chain length.

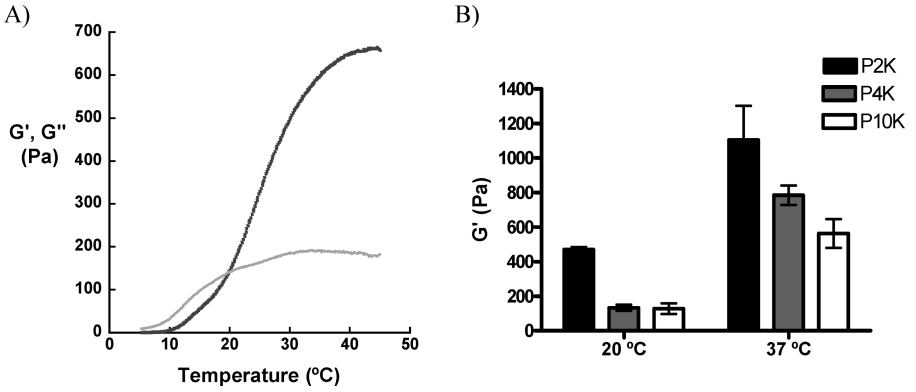

Figure 4. (A) Typical curve of storage modulus (G', in black) and loss modulus (G'', in gray) as a function of temperature (30 wt % P10K at pH 5). (B) Storage moduli of 30 wt % hydrogels at 20 and 37 °C at pH 5. Values are given as mean ± standard deviation; $n = 3$.

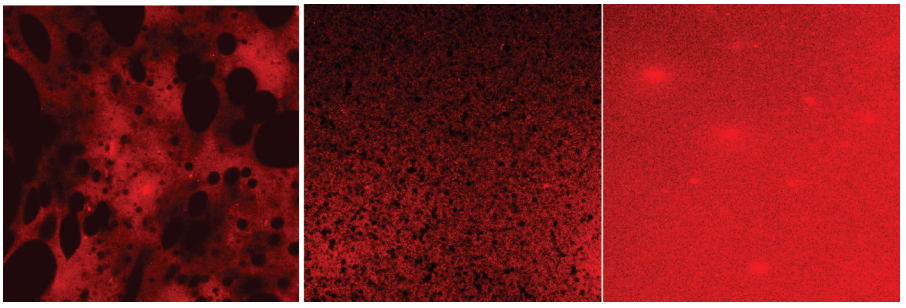

Figure 5. Confocal laser scanning microscopy pictures of 20 wt % gel at pH 5 (P2K, P4K, and P10K from left to right) containing trace amounts of Nile Red. Bright red spots originate from incompletely dissolved Nile Red. Scale of pictures 65 μm × 65 μm.

percentage of the polymers was the same in all the gels, the molar concentration of the P2K gels was about 30% higher than the molar concentration of the P10K gels due to the difference in molecular weight of the polymers. Although this seems the most logical explanation for the stronger P2K gels, there might be other factors playing a role in the origin of the gel strength. The hydrophilic PEG/thermosensitive ratio of the P2K polymers is much smaller, as suggested by their cloudy appearance at high temperatures compared to the other compositions. The P2K hydrogels also expelled a small percentage of water upon gel formation, which was not observed for the P4K and P10K hydrogels. Apparently, the self-assembly process of these thermosensitive triblock polymers is significantly affected by hydrophilic PEG content.

Confocal Laser Scanning Microscopy and Cryo-SEM of Hydrogels. To gain more insight into gel structure, confocal laser scanning microscopy (CLSM) pictures of the gels were taken after mixing with Nile Red to stain the hydrophobic domains. Figure 5 displays stained 20 wt % gels of P2K, P4K, and P10K. Phase separation was clearly visible in the P2K and P4K gels, with hydrophilic domains (black) surrounded by a hydrophobic (red) environment. To confirm that the black domains were indeed hydrophilic, fluorescently labeled streptavidin was mixed with a P2K solution and heated to room temperature. A CLSM picture showed the fluorescent signal in the opposite domains as compared to the Nile Red colored samples (see Supporting Information).

A clear trend in the extent of phase separation in the gels was found with respect to the hydrophilic PEG content in the polymers in the CLSM experiments. The size and heterogeneity of the hydrophilic domains decreased with increasing

PEG block length, and phase separation was not discernible for P10K hydrogels.

Similar domains were visualized using cryo-SEM measurements (Figure 6). Again, two types of domains are visible: a polymer-rich domain showing a typical polymer gel network and dark domains in which no structure was observed. Experiments on P2K samples at 25 and 37 °C showed that the phase separation was temperature-dependent (see Supporting Information). However, a kinetic contribution to this phase separation cannot be excluded because the samples were only maintained for 5 min at a given temperature.

The observed phase separation in both CLSM and cryo-SEM measurements can explain the differences found in macromolecular diffusion within these gels as shown in the earlier FRAP section. The labeled dextrans are hydrophilic and are expected to localize mainly in the water-rich/polymer-poor domains and are minimally restricted in their mobility within these domains. Going from P2K to P4K and P10K gels, the degree of phase separation probably decreases and domains become smaller. The mobility of the dextrans then becomes more restricted, resulting in lower diffusion coefficients.

Trends in mechanical properties can also be explained by this phase separation mechanism. For P2K gels, the overall polymer-rich phase is smaller in volume (due to large water-rich domains), and therefore the polymer concentration is much higher in these domains than in the P4K and P10K hydrogels. The water-rich phase will not contribute much to hydrogel strength, but the high polymer concentration across the rest of the gel results in a high overall elastic modulus.

Although the observations of the different experiments are consistent, a more complete explanation of the origin of the phase separation is desired. If self-assembly of the thermosensitive outer blocks were the only driving force for gel formation, then a homogeneous gel network throughout the whole sample would be expected. The outer blocks will assemble in hydrophobic domains with a size similar to the hydrophobic core of a polymeric micelle, and these hydrophobic domains will be linked via the hydrophilic middle blocks of the polymer (network of connected micelles).[35−38] However, this explanation is not sufficient to clarify the phase separation on much larger length scales as seen in the CLSM and cryo-SEM pictures. As shown by Pham et al., solutions of associative triblock polymers can undergo phase separation into a dilute micellar "gas" phase and a polymer-rich "liquid" phase consisting of a network of interconnected micelles.[39] A similar phase separation seems to occur in our materials: two distinct regions with different polymer concentrations were found (Figure 5A−C). No effect of the heating rate was found on the FRAP curves or rheological properties. Only for the P2K gel in CLSM measurements, smaller hydrophilic domains were found upon heating the sample quickly compared to slow heating (see Supporting Information). Similar phase separations have been demonstrated in other self-assembling thermosensitive hydrogels based on poly(*N*-isopropylacrylamide) and other amphiphilic systems.[40,41] The hydrophilic−hydrophobic balance plays an important role in the phase separation process together with a tendency to expel water.[42] This is also the case in our gel system; for P2K polymers the hydrophobic−hydrophilic ratio was highest, and they gave the most phase-separated gels.

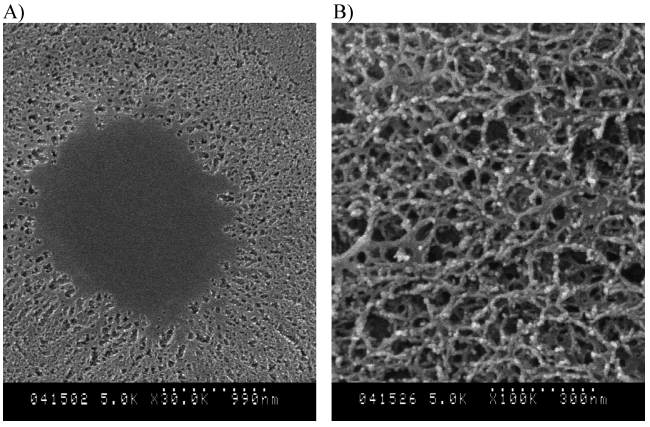

Figure 6. Cryo-SEM pictures of two different domains in 20 wt % P2K gels at pH 5 (A) and porous polymer-rich network structure (B). Scale bars: (A) 990 nm; (B) 300 nm.

Degradation of Hydrogels. Figure 7 displays the mobile fraction of FD70 molecules in P4K gels at two different time points. Fluorescence recovery curves were measured immediately after film formation as above, and the same gels were incubated at 37 °C for 1 week in the presence of excess buffer to keep pH constant. After 1 week, the FRAP curves of these gels were measured again. These experiments were performed at both pH 5 and pH 7.5. At pH 5 ester hydrolysis is minimized,[20] and pH 7.5 was chosen to mimic degradation rates in physiological conditions. At pH 5, the mobile fraction did not increase significantly after 1 week. However, at pH 7.5 the mobile fraction increased in time for all measured temperatures, suggesting hydrogel degradation leading to an increased hydrophilicity of the gel, which in turn translates in an increased mobility of the entrapped dextrans. Such biodegradation is important for injectable systems, since it provides a means to compensate for decreased diffusional release as drug becomes depleted and since it obviates the need to remove the vehicle after release.

The pH-dependent degradation indicates that ester hydrolysis is the responsible process for degradation. The polymers used in this study contain several ester bonds that can be hydrolyzed in aqueous environment. The ester bonds are located between the PEG and thermosensitive blocks in the

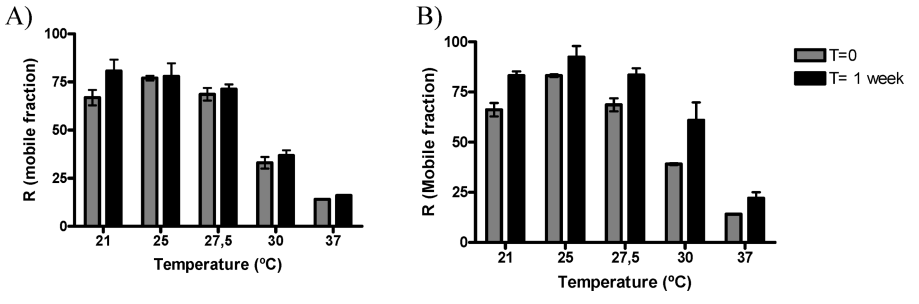

Figure 7. Mobile fraction of FD70 in 30% (w/w) P4K gels at pH 5 (A) and at pH 7.5 (B). Data are shown as mean ± standard deviation; $n = 3$.

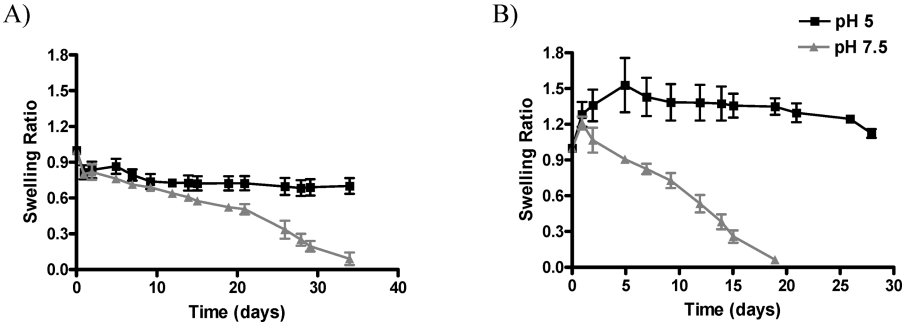

Figure 8. Degradation/swelling of thermosensitive hydrogels: (A) 30 wt % P2K gels; (B) 30 wt % P4K gels at pH 5.0 (black squares) or at pH 7.5 (gray triangles). Data are shown as mean ± standard deviation; $n = 3$.

main chain, but they are more abundant in the lactic acid side chains of the thermosensitive outer blocks of the polymers. When these side chains are hydrolyzed, the polymer becomes more hydrophilic, resulting in an increase in the cloud point. As the diffusion of entrapped molecules is dependent on the temperature as shown in Figure 1, an increase in mobility of these molecules was expected and also found upon degradation of the hydrogel.

Degradation of the hydrogels was followed by incubating them at 37 °C in excess of buffer and by measuring the gel weight at several time points. Figure 8 shows the swelling P2K and P4K gels at pH 5 and pH 7.5. P2K is the polymer with the overall highest hydrophobicity, and the swelling ratio dropped immediately to a value just below 1 due to expulsion of water from the gel. This phenomenon disappeared with increasing PEG chain length and consequently polymer hydrophilicity. For P10K the swelling ratio could not be measured because the gels swelled very quickly, resulting in a fast decrease in polymer concentration and loss of gel properties, as was found previously.[43] As can be seen, the P2K and P4K gels were stable for a long time at pH 5. After some initial swelling for P4K gels, the gel weight was stable for over 30 days. At physiological pH the gels degraded in time. The more hydrophobic P2K gels were fully degraded in 30−35 days, while the more hydrophilic P4K gels degraded faster within 20 days.

Concluding Remarks

In this paper, we described the diffusion of macromolecules through self-assembling ABA triblock polymer hydrogels. These hydrogels are suitable as *in situ* gelling systems for controlled delivery of biotherapeutics because of their mild preparation procedure, simple encapsulation of macromolecules, tunable diffusion properties, and biodegradability.

Mobility of entrapped molecules depended on probe molecular weight, temperature, and the characteristics of the polymer. The length of the hydrophilic PEG middle block had a notable effect on hydrogel properties. The storage modulus of the gels increased with decreasing hydrophilic content in the polymers. CLSM and cryo-SEM measurements showed that the gels were phase-separated into polymer-poor hydrophilic and polymer-rich hydrophobic domains, and the extent of phase separation could also be controlled by the PEG block length in the polymers.

One might expect, based on theories of diffusion in inhomogenous media, that the degree of phase separation and the structure of domains will have a strong impact on transport in the hydrogels. Techniques described here, such as LCSM and cryo-SEM, may therefore be useful in the future in elucidating the relationship between mesostructure and transport. Insofar as the mesostructures change depending on thermal history and degradation of the triblock copolymers, it would be interesting to utilize these techniques to provide "snapshots" of structural change over time.

Acknowledgment. This research was supported by the Dutch Program for Tissue Engineering (DPTE) (Project 6731) and the National Institutes of Health (Grant HD040366). We thank Prof. Victor Bloomfield (University of Minnesota) for donation of the FRAP apparatus.

Supporting Information Available: Confocal laser scanning microscopy pictures of fluorescent streptavidin and Nile Red in P2K gels after quick and slow heating and cryo-SEM of P2K samples at 25 and 37 °C. This material is available free of charge via the Internet at http://pubs.acs.org.

References and Notes

(1) Hennink, W. E.; Van Nostrum, C. F. *Adv. Drug Delivery Rev.* **2002**, *54*, 13–36.
(2) Khutoryanskiy, V. V. *Int. J. Pharm.* **2007**, *334*, 15–26.
(3) Van Tomme, S. R.; Van Steenbergen, M. J.; De Smedt, S. C.; Van Nostrum, C. F.; Hennink, W. E. *Biomaterials* **2005**, *26*, 2129–2135.
(4) Lee, K. Y.; Rowley, J. A.; Eiselt, P.; Moy, E. M.; Bouhadir, K. H.; Mooney, D. J. *Macromolecules* **2000**, *33*, 4291–4294.
(5) Vermonden, T.; Besseling, N. A. M.; Van Steenbergen, M. J.; Hennink, W. E. *Langmuir* **2006**, *22*, 10180–10184.
(6) Vermonden, T.; Van Steenbergen, M. J.; Besseling, N. A. M.; Marcelis, A. T. M.; Hennink, W. E.; Sudhölter, E. J. R.; Cohen Stuart, M. A. *J. Am. Chem. Soc.* **2004**, *126*, 15802–15808.
(7) van de Mannaker, F.; van der Pot, M.; Vermonden, T.; van Nostrum, C. F.; Hennink, W. E. *Macromolecules* **2008**, *41*, 1766–1773.
(8) Van Tomme, S. R.; Storm, G.; Hennink, W. E. *Int. J. Pharm.* **2008**, *355*, 1–18.
(9) Hoffman, A. S. *Adv. Drug Delivery Rev.* **2002**, *43*, 3–12.
(10) Ruel-Gariépy, E.; Leroux, J.-C. *Eur. J. Pharm. Biopharm.* **2004**, *58*, 409–426.
(11) Xu, C.; Kopecek, J. *Polym. Bull.* **2007**, *58*, 53–63.
(12) Jeong, B.; Gutowska, A. *Trends Biotechnol.* **2002**, *20*, 305–311.
(13) Petka, W. A.; Harden, J. L.; McGrath, K. P.; Wirtz, D.; Tirrell, D. A. *Science* **1998**, *281*, 389–392.
(14) Peppas, N. A.; Huang, Y.; Torres-Lugo, M.; Ward, J. H.; Zhang, J. *Annu. Rev. Biomed. Eng.* **2000**, *2*, 9–29.
(15) Tomić, K.; Veeman, W. S.; Boerakker, M.; Litvinov, V. M.; Dias, A. A. *J. Pharm. Sci.* **2008**, *97*, 3245–3256.
(16) Klouda, L.; Mikos, A. G. *Eur. J. Pharm. Biopharm.* **2008**, *68*, 34–45.
(17) Jeong, B.; Kim, S. W.; Bae, Y. H. *Adv. Drug Delivery Rev.* **2002**, *54*, 37–51.
(18) Censi, R.; Vermonden, T.; van Steenbergen, M. J.; Deschout, H.; Braeckmans, K.; De Smedt, S. C.; van Nostrum, C. F.; di Martino, P.; Hennink, W. E. *J. Controlled Release* **2009**, in press (DOI: 10.1016/j.jconrel.2009.06.003).
(19) Soga, O.; Van Nostrum, C. F.; Hennink, W. E. *Biomacromolecules* **2004**, *5*, 818–821.
(20) Neradovic, D.; Van Steenbergen, M. J.; Vansteelant, L.; Meijer, Y. J.; Van Nostrum, C. F.; Hennink, W. E. *Macromolecules* **2003**, *36*, 7491–7498.

(21) Jacobson, K.; Wu, E.; Poste, G. *Biochim. Biophys. Acta* **1976**, *433*, 215–222.
(22) Busch, N. A.; Kim, T.; Bloomfield, V. A. *Macromolecules* **2000**, *33*, 5932–5937.
(23) Jena, S. S.; Bloomfield, V. A. *Macromolecules* **2005**, *38*, 10551–10556.
(24) Jena, S. S.; Bloomfield, V. A. *Macromolecules* **2005**, *38*, 10557–10560.
(25) De Smedt, S. C.; Meyvis, T. K. L.; Demeester, J.; Van Oostveldt, P.; Blonk, J. C. G.; Hennink, W. E. *Macromolecules* **1997**, *30*, 4863–4870.
(26) Tong, J.; Anderson, J. L. *Biophys. J.* **1996**, *70*, 1505–1513.
(27) Alvarez-Mancenideo, F.; Braeckmans, K.; De Smedt, S. C.; Demeester, J.; Landin, M.; Martinez-Pacheco, R. *Int. J. Pharm.* **2006**, *316*, 37–46.
(28) Tolentino, T. P.; Wu, J.; Zarnitsyna, V. I.; Fang, Y.; Dustin, M. L.; Zhu, C. *Biophys. J.* **2008**, *95*, 920–930.
(29) Roth, D. M.; Harper, I.; Pouton, C. W.; Jans, D. A. *J. Cell. Biochem.* **2009**, *107*, 1160–1167.
(30) Branco, M. C.; Pochan, D. J.; Wagner, N. J.; Schneider, J. P. *Biomaterials* **2009**, *30*, 1339–1347.
(31) Neradovic, D.; Van Nostrum, C. F.; Hennink, W. E. *Macromolecules* **2001**, *34*, 7589–7591.
(32) Lanz, E.; Gregor, M.; Slavík, J.; Kotyk, A. *J. Fluoresc.* **1997**, *7*, 317–319.
(33) Masters, J. I. *J. Chem. Phys.* **1955**, *23*, 1865–1874.
(34) Apkarian, R. P.; Wright, E. R.; Seredyuk, V. A.; Eustis, S.; Conticello, V. P.; Menger, F. M. *Microsc. Microanal.* **2003**, *9*, 286–295.
(35) Sanabria-DeLong, N.; Crosby, A. J.; Tew, G. N. *Biomacromolecules* **2008**, *9*, 2784–2791.
(36) Li, C.; Madsen, J.; Armes, S. P.; Lewis, A. L. *Angew. Chem., Int. Ed.* **2006**, *45*, 3510–3513.
(37) Semenov, A. N.; Joanny, J.-F.; R, K. A. *Macromolecules* **1995**, *28*, 1066–1075.
(38) Lee, D. S.; Shim, M. S.; Kim, S. W.; Lee, H.; Park, I.; Chang, T. *Macromol. Rapid Commun.* **2001**, *22*, 587–592.
(39) Pham, Q. T.; Russel, W. B.; Thibeault, J. C.; Lau, W. *Macromolecules* **1999**, *32*, 2996–3005.
(40) Annaka, M.; Matsuura, T.; Yoshimoto, E.; Taguchi, H.; Sasaki, S.; Sugiyama, M.; Hara, Y.; Okano, T. *Colloids Surf., B* **2004**, *38*, 201–207.
(41) Zhang, R.; Li, W.; Li, K.; Lu, C.; Zhan, L.; Ling, L. *Microporous Mesoporous Mater.* **2004**, *72*, 167–173.
(42) Nayak, S.; Debord, S. B.; Lyon, L. A. *Langmuir* **2003**, *19*, 7374–7379.
(43) Vermonden, T.; Fedorovich, N. E.; van Geemen, D.; Alblas, J.; van Nostrum, C. F.; Dhert, W. J. A.; Hennink, W. E. *Biomacromolecules* **2008**, *9*, 919–926.